

# Optimizing LLM Inference for Database Systems: Cost-Aware Scheduling for Concurrent Requests

Kyoungmin Kim

EPFL

Switzerland

kyoung-min.kim@epfl.ch

Caglar Gulcehre

EPFL

Switzerland

caglar.gulcehre@epfl.ch

Kijae Hong

CERES TECHNOLOGIES

South Korea

kjhong@cerestechs.com

Anastasia Ailamaki

EPFL

Switzerland

anastasia.ailamaki@epfl.ch

## ABSTRACT

LLMs are increasingly used inside database systems and in database applications for better complexity management and decision-making, where LLM inferences require significant GPU costs. LLM inference systems, however, are slow compared to database systems, limiting the expansion of the use of LLMs inside database systems. This paper first analyzes the LLM inference performance and focuses on a data management issue in LLM inference. We reveal that the root of the problem is the lack of an adequate resource cost model and optimization strategy when executing multiple concurrent inference requests. We adapt classic database multi-query optimization techniques by introducing cost models for concurrent inference requests and new scheduling strategies to optimize the use of memory resources by concurrent requests, thereby substantially improving performance.

## PVLDB Reference Format:

Kyoungmin Kim, Kijae Hong, Caglar Gulcehre, and Anastasia Ailamaki. Optimizing LLM Inference for Database Systems: Cost-Aware Scheduling for Concurrent Requests. PVLDB, 14(1): XXX-XXX, 2020.

doi:XX.XX/XXX.XX

## PVLDB Artifact Availability:

The source code, data, and/or other artifacts have been made available at URL\_TO\_YOUR\_ARTIFACTS.

## 1 INTRODUCTION

Unlike LLM training, which is a one-time cost, LLM inference is an ongoing and significantly more expensive process due to high GPU costs and energy consumption. For instance, ChatGPT receives approximately 600 million visits per month<sup>1</sup>, incurring GPU expenses exceeding \$20 million monthly<sup>2</sup>. Recent advancements, such as OpenAI's o1/o3 models and Deep Research<sup>3</sup>, further underscore the

This work is licensed under the Creative Commons BY-NC-ND 4.0 International License. Visit <https://creativecommons.org/licenses/by-nc-nd/4.0/> to view a copy of this license. For any use beyond those covered by this license, obtain permission by emailing info@vlldb.org. Copyright is held by the owner/author(s). Publication rights licensed to the VLDB Endowment.

Proceedings of the VLDB Endowment, Vol. 14, No. 1 ISSN 2150-8097.

doi:XX.XX/XXX.XX

<sup>1</sup><https://explodingtopics.com/blog/chatgpt-users>

<sup>2</sup><https://seo.ai/blog/how-many-users-does-chatgpt-have>,

<https://www.semianalysis.com/p/the-inference-cost-of-search-disruption>

<sup>3</sup>[https://openai.com/index/introducing-deep-research/?utm\\_source=chatgpt.com](https://openai.com/index/introducing-deep-research/?utm_source=chatgpt.com)

rising demands of LLM inference, as these models extend inference time to enhance reasoning capabilities. Meanwhile, open-source models like Llama and DeepSeek enable broader adoption of LLM inference. Reducing LLM inference latency is thus crucial for both economic and environmental sustainability, given the substantial CO<sub>2</sub> emissions associated with GPU usage [25, 34].

LLMs are also increasingly used inside database systems and in database applications. For instance, they are used in complex data management [8, 28], database administration [42, 53], and tasks such as query optimization [4, 21] and natural language to SQL translation [36]. Analytical queries also extend relational algebra to call LLMs, such as filtering, joining, and ordering rows with natural language predicates [33], to provide a semantically rich data processing.

As the demand for LLMs grows, researchers and developers focus on designing more efficient inference systems [17, 18, 32, 44, 45, 52, 54]. However, these efforts often involve redesigning and reconstructing entire systems, for example, overlapping GPU computations and data transfers to reduce latency [54]. This approach is labor- and hardware-intensive, requiring extensive analysis, implementation, and GPU usage. Moreover, it remains unclear whether existing systems are fully utilized, potentially leaving untapped optimization opportunities. A more cost-effective, goal-oriented approach is needed instead of relying on a naive trial-and-error process.

Furthermore, LLM inference systems are still much slower than database systems, limiting the efficiency of database applications and prohibiting the expansion of the use of LLMs inside. For example, retrieving top-k rows and joining two tables using LLMs are thousands of times slower than vector similarity-based top-k search and joins [33], which are already slower than typical relational operations. This paper first analyzes and optimizes the general LLM inference performance before delving into tailored database scenarios.

Efficient data management is central to LLM inference, a challenge we illustrate through an analogy with database query processing. An inference request functions similarly to a recursive query, where each iteration generates a new token. Within each iteration, operations such as attention mechanisms [11, 43] and matrix multiplications resemble database operators, with intermediate data stored in GPU memory and reused in subsequent iterations

alongside model weights (detailed in Section 2). To optimize efficiency, multiple concurrent requests are batched at each iteration, amortizing the cost of loading model weights into memory [45]. However, the resulting contention for limited GPU memory necessitates batching and scheduling strategies that selectively evict and reschedule requests [3].

Despite the aforementioned similarities, two critical components, which are omnipresent in database systems, are missing from LLM inference systems: (a) a comprehensive cost model for each batch of requests and (b) a multi-query optimization (scheduling LLM requests in our analogy) utilizing the cost model. Instead, LLM inference systems basically use naive *first-come-first-serve* scheduling techniques [3, 17], and the resulting (suboptimal) schedules can increase latency by more than a factor of six [2].

To address this gap, this paper proposes INFERMAX, a framework that facilitates the development and analysis of LLM inference through three key components: (1) a simple yet effective cost model for predicting batch processing times, (2) a unified scheduler that generalizes existing approaches and extends beyond them, and (3) the formulation of an optimal scheduling problem as a *Constraint Satisfaction Problem (CSP)* for the first time, which serves as a performance bound for scheduling. INFERMAX is implemented on top of an LLM inference simulator [1], eliminating the need for GPUs during development, except for a few hours required for learning cost models. This enables extensive analysis to derive insights and hypotheses for improved scheduling policies without direct GPU usage. The discovered hypotheses can be validated through CSP, ensuring that observed performance gains are not incidental. CSP further allows for the theoretical assessment of new policies before committing resources to their implementation.

Extensive analysis using INFERMAX reveals a counterintuitive insight: allowing request evictions can improve performance more than strictly avoiding them, particularly for short requests under high memory contention. The reason is that selective evictions enable better utilization of GPU memory and computation capacity. Therefore, we introduce a simple yet effective scheduling policy that prioritizes evictions of short requests to optimize resource allocation, resulting in up to a 1.4x decrease in latency for our analysis workloads without regression. We deploy this to a popular LLM inference system, vLLM [17], and achieve a 1.2x decrease for a real-world workload, where an estimated performance bound with unlimited memory is 1.4x. These improvements demonstrate the potential for significant economic and environmental savings in general LLM inference operations, for example, more than \$2.8 million per month for ChatGPT. In summary, this paper

- addresses a data management problem in LLM inference (Section 2);
- introduces INFERMAX to facilitate cost-effective development and analysis of LLM inference schedulers based on a cost model and unified scheduler on top of a simulation framework (Section 3);
- provides an extensive analysis (worth more than 250 GPU hours) of different schedulers, including the ones in LLM systems and our own, for assessing the feasibility of scheduling policies and predicting their performance upper bounds (Section 4);

- proposes a novel formulation of optimal scheduling as CSP which acts as a performance bound and proof-by-example approach for proving the hypotheses found in the analysis (Section 5); and
- based on the insights from the analysis proposes a straightforward and efficient scheduling strategy, which can substantially save GPU costs in the real world (Section 6).

## 2 BACKGROUND

This section explains the data management and processing in LLM inference.

### 2.1 Processing a Single LLM Request

In LLM inference, the input text of a request is called *prompt*. The inference system first processes input tokens to generate a new token, a phase known as *prefill*. This is followed by *decode* steps, where each step generates a new token based on the last generated one, until the end-of-sequence (EOS) token is generated (e.g., how the request R1 in Figure 1 is processed at each step or batch) or a predefined output length is reached. The model’s context size  $C$  (at least few thousands) also limits the maximum length.

At each step, after embedding the input tokens into vector representations, each model layer executes GPU-based operators including activations and matrix multiplications between input vectors and model weights. The output vectors have the same size with the input vectors. It then feeds the final layer’s output to a sampling component to generate the next token.

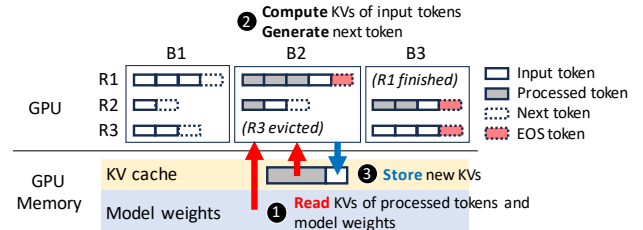


Figure 1: Data management and processing in LLM inference. R and B denote a request and batch. Circled numbers show the three steps occurring batch-wise. If the KV cache size is 8, R3 is evicted in B2 as the processed tokens of R1 to R3 would otherwise be  $4+2+3 > 8$  after processing B2.

Most LLMs rely on the Transformer architecture with *attention* mechanism [43], which complicates the data management in LLM inference. Non-attention operators such as matrix multiplications and activations process tokens (or their vectors) independently, requiring  $N$  input vectors for  $N$  tokens and generating  $N$  output vectors of the same size. Therefore, these use only a fixed amount of GPU memory. In contrast, attention operator requires a larger input data, i.e.,  $\Omega(N)$ . This attributes to computing the attention score for each input token and *all* previous tokens in the request. Let  $Q_i$ ,  $K_i$ , and  $V_i$  be the query, key, and value vectors of the  $i$ -th token in the request. When processing the  $i$ -th token, the attention score depends on  $Q_i$ ,  $K_1$  to  $K_i$ , and  $V_1$  to  $V_i$  with  $O(i)$  time complexity.

Please refer to [43] for detailed computations. This attention lies in every model layer, and query/key/value vectors are different across layers even for the same token.

Since  $K_i$  and  $V_i$  are used in processing any subsequent token, key-value (KV) caching [9] stores previously computed KVs in GPU memory (gray region in the KV cache in Figure 1), allowing the system to avoid recomputing them every step. This is widely adopted for efficient LLM inference, as reading KVs from the memory is typically faster than recomputing KVs for existing GPU-model configurations considering the GPU bandwidth/FLOPs and vector sizes.

In this structure, prefill steps lack KVs to read as no token has been processed, and processing the first  $i$  tokens requires quadratic  $- O(1+2+\dots+i) = O(i^2)$  – complexity. These make prefills *compute-bound*. In contrast, decode steps have an expanding set of KVs to read as output length grows, causing decode steps to become increasingly *memory-bound* [3].

## 2.2 Processing Multiple LLM Requests

The complexity of data management increases for multiple requests. While the most efficient way would be to process all requests simultaneously at each step to amortize the cost of loading model weights to GPUs, this is infeasible due to the large memory demand of attention operators. LLM inference systems selectively schedule requests at each step as in Figure 1 under limited GPU memory, particularly the maximum KV cache size,  $M$ , in terms of the number of KVs (less than millions). This is determined by the remaining GPU memory after loading model weights onto memory.  $C$  also limits the total number of tokens to process per batch.

To improve inference efficiency, systems adapt techniques from databases and operating systems. Continuous batching [45] schedules new requests step-by-step as resources become available, avoiding idle waiting times, similarly to pipelining. Paged attention [17] enhances memory utilization by managing KVs in page segments rather than reserving large allocations per request, say  $C$ . Figure 1 also adopts these. Hybrid batching [3] simply allows both prefill- and decode-phase requests can be batched together, though prefills, due to large prompts, often consume more resources and can delay decode-phase requests in the same batch. Chunked prefill [3] mitigates this delay by partially processing prompts, reducing prefill time per batch. A parameter  $P$  (where  $P \leq C$ ) sets the maximum number of prefill tokens per batch. If a subset of prompt tokens have been processed, subsequent chunked prefills need to read KVs of those tokens. A new token can only be generated once all prompt tokens are processed. In the remainder of the paper, we assume that all mentioned techniques are enabled by default.

We define two metrics to explain scheduling results: batch size, representing the number of requests in each batch, and running size, indicating the number of active (running) requests holding KVs. When the total number of KVs of running requests reaches  $M$ , the system needs to preempt or evict some requests, releasing their KVs. Once evicted, a request's generated tokens are appended to the prompt. We call processing these tokens again as the *refill* phase. In Figure 1, R3 is evicted at B2 and refilled at B3. Notably, KVs are recomputed during the refill, rather than offloaded to other storage and reloaded, as PCIe bandwidth between GPU and external storage is lower than the GPU's processing capacity [17].

## 3 INFERMAX

This section introduces INFERMAX, our analytical framework that facilitates cost-effective development and analysis of LLM inference, illustrated in Figure 2. Given a system configuration and test workload, schedulers that are deployable to inference systems generate schedules (1), which can be run by an LLM inference system (2) to measure actual performance on GPUs. However, each test run can take hours [5], and running every schedule on GPUs may further increase computational costs. Long, complex workloads with varying input and output sizes also make it hard to understand the behaviors of schedulers and discover any insights for improving them.

To address these, we use a separate set of workloads for analysis and adopt an alternative simulation-based approach to minimize using actual GPUs. First, we obtain profiling results of GPU times on simple workloads and use them to train cost models (3). To avoid confusion with LLMs, we always prepend "cost." The cost models predict batch execution times based on the number of tokens to process and KVs to read. Here, one may use theoretical hardware bounds, such as those used in [46], as theoretical cost models. We do not focus on them in this study.

Then, along with deployable schedulers, we implement *hypothetical* schedulers to measure the performance upper bounds of certain scheduling policies. We call hypothetical since these schedulers can utilize all information of the analysis workload. For example, we use eviction-free schedulers in Section 4 that reserve maximum memory usage for each request to avoid evictions. Since knowing the maximum use requires knowing the requests' output sizes in advance, they cannot be deployed for real-world workloads. The output schedules and cost models are used to estimate the performance (4). Finally, the cost models can further be calibrated from the actual performance obtained from inference systems (5).

Our formulation of finding optimal schedules into constraint satisfaction problem (CSP) in Section 5 can be regarded as a special case of hypothetical schedule(r). It requires knowing the input and output sizes of requests, as well as the cost models to set optimization objectives, such as minimizing the total latency.

For our system configuration, we can simulate a single GPU for small models (e.g., 7B in Section 4) but also scale to multiple GPUs for large models (e.g., 70B in Section 6). Still, we focus on a single instance (or replica) setup with a single model and request pool. Supporting multiple instances with separate models and request pools is straightforward as the requests are typically routed to instances in a simple round-robin fashion [1, 17]. Therefore, the multi-instance setup exhibits similar performance characteristics with the single-instance setup. While one can further formulate finding optimal routing problem into CSP, we leave it as a future work.

### 3.1 Unified Algorithm for Schedulers

This section details a unified algorithm (Algorithm 1) that captures various schedulers, including the ones deployed in LLM inference systems and our hypothetical schedulers in Figure 2 knowing the future information such as output lengths.

Algorithm 1 repeatedly fetches new arrived requests (Line 4), thereby supporting online workloads with continuously arriving

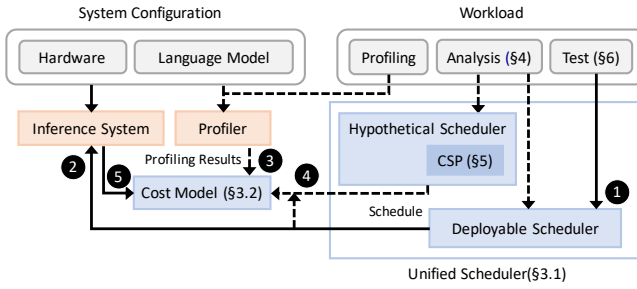


Figure 2: Overview of INFERMAX. Solid/dashed arrows indicate deployment/development phase. Orange boxes require actual GPUs while blue boxes do not. CSP denotes constraint satisfaction problem, and there is an omitted arrow from the cost model to CSP.

requests. It then forms a batch (Line 5), processes all requests in the batch (Line 6), and appends the incomplete requests back to the running requests (Line 7). In our simulation, Line 6 does not perform GPU operators but estimates batch execution times from cost models.

Schedulers vary in the implementation of `GETNEXTBATCH`, particularly in steps 1-4. The requests in  $\mathcal{R}_w$  and  $\mathcal{R}_r$  are first ordered and grouped by certain priority functions, e.g., arrival time, (Line 11, 1). For each group  $\mathcal{G}$  of requests and its candidate request  $cand$ , if hybrid batching is disabled and  $cand$  is in a different phase (prefill or decode) than the requests already in  $\mathcal{B}$ ,  $cand$  is skipped (2). In step 3, `CANALLOCATE` checks if  $cand$  can be added to  $\mathcal{B}$  based on the following conditions:

- $C$ : Check  $cand.c \leq C - \sum_{r \in \mathcal{B}} r.c$ ;  $r.c$  denotes the number of tokens to process for a request  $r$ . This ensures that the total number of tokens to process in this batch does not exceed  $C$ .
- $P$ : If  $cand$  is in the prefill phase, check  $cand.c \leq P - \sum_{r \in \mathcal{B}} r.c$  where  $P \leq C$ .
- $M$ : Check  $cand.m_{reserve} \leq M - \sum_{r \in \mathcal{R}_r} r.m$ ;  $r.m$  denotes the number of processed tokens or KVs in KV cache for a request  $r$ , and  $m_{reserve}$  is the number of KVs to reserve (typically 1 for decode and input size for prefill).

For chunked prefill,  $cand.c$  can be adjusted to a smaller value,  $\min(cand.c, P - \sum_{r \in \mathcal{B}} r.c)$ , if  $cand$  is in prefill phase. If allocation fails due to insufficient  $M$ , the scheduler opts to evict other running requests in lower-priority requests to release their KVs and reassess  $cand$  (4). If no such request remains,  $cand$  is self-evicted. Once evicted, other candidates in the same group can be probed or skipped. If allocation fails for other reasons, no eviction occurs. Any evicted request is removed from  $\mathcal{R}_r$  and appended to  $\mathcal{R}_w$ . If  $cand$  is successfully allocated, it is added to  $\mathcal{B}$  and removed from its original queue (Line 17).

We explain the algorithm with two representative schedulers from vLLM [17] and SARATHI [3] as they are by default enabled in LLM inference systems and show better performance than other previous schedulers [1, 30, 31, 45]. In vLLM, the requests are organized into two groups,  $\mathcal{R}_w$  and  $\mathcal{R}_r$ , with priority given to  $\mathcal{R}_w$  with prefill/refill requests only (1). Hybrid batching and chunked prefill are disabled for vLLM (2 and 3). If memory  $M$  is insufficient for

allocation in 3, vLLM skips to the next group if the current group is  $\mathcal{R}_w$ , and evicts lower-priority requests if the group is  $\mathcal{R}_r$  in 4. SARATHI, on the other hand, creates three groups:  $\mathcal{R}_r^d$ ,  $\mathcal{R}_r^p$ , and  $\mathcal{R}_w$ , where  $\mathcal{R}_r^d$  and  $\mathcal{R}_r^p$  represent running requests in the decode and prefill phases. This setup prioritizes decode requests in contrast to vLLM (1), and both hybrid batching and chunked prefill are enabled (2 and 3). If  $M$  is insufficient in 3, SARATHI evicts requests if the current group is  $\mathcal{R}_r^d$  and skips if the group is  $\mathcal{R}_w$  in 4; for  $\mathcal{R}_r^p$ , all requests can be allocated as they are in the middle of prefill and have already reserved the whole input tokens.

### Algorithm 1. SCHEDULER( $M, C, P$ )

---

**Input:** Max KV cache size  $M$ , max # tokens per batch  $C$ , max # prefill tokens per batch  $P$

```

1:  $\mathcal{R}_w \leftarrow \emptyset$  /* queue of waiting requests */  

2:  $\mathcal{R}_r \leftarrow \emptyset$  /* queue of running requests */ /*/  

3: while (true) do  

4:    $\mathcal{R}_w \leftarrow \mathcal{R}_w \cup \text{GETNEWREQUESTS}()$  /* schedule batch  $\mathcal{B}$  from  $\mathcal{R}_w \cup \mathcal{R}_r$  */  

5:    $\mathcal{B} \leftarrow \text{GETNEXTBATCH}(\mathcal{R}_w, \mathcal{R}_r, M, C, P)$  /* Process  $\mathcal{B}$ , send outputs to users, remove completed requests from  $\mathcal{B}$  */  

6:    $\mathcal{B}' \leftarrow \text{PROCESS}(\mathcal{B})$  /* append remaining  $\mathcal{B}'$  to  $\mathcal{R}_r$  */  

7:    $\mathcal{R}_r \leftarrow \mathcal{R}_r \cup \mathcal{B}'$   

8: Function: GETNEXTBATCH( $\mathcal{R}_w, \mathcal{R}_r, M, C, P$ )  

9: begin  

10:   $\mathcal{B} \leftarrow \emptyset$  /* batch of requests */  

11:  foreach ( $\mathcal{G} \in \text{GROUPREQUESTS}(\mathcal{R}_w \cup \mathcal{R}_r)$ ) 1 do /*/  

12:    foreach ( $cand \in \mathcal{G}$ ) do  

13:      CHECKHYBRIDBATCHING 2  

14:      while ( $\neg \text{CANALLOCATE}(cand, \mathcal{B}, M, C, P)$ ) 3 do  

15:        EVICTLOWERPRIORITYREQUEST 4  

16:      else  

17:         $\mathcal{B} \leftarrow \mathcal{B} \cup \{cand\}$ , REMOVEREQUEST( $cand, \mathcal{R}_w, \mathcal{R}_r$ )  

18: return  $\mathcal{B}$ 

```

---

## 3.2 Cost Models for Batch Times

This section explains the cost models used for estimating batch times. Figure 3 illustrates examples of GPU processing times for various operators within a model layer (corresponds to 3 in Figure 2). Figure 3(a) shows the total time required for non-attention operators, such as matrix multiplications and activations, which depend on the number of tokens processed in a batch,  $\sum_{r \in \mathcal{B}} r.c$ . Figure 3(b) presents the time for decode-phase attention, determined by the number of KVs read from the cache,  $\sum_{r \in \mathcal{B}} r.m$ . In contrast, prefill-attention time in Figure 3(c) scales with the square of the number of tokens processed,  $\sum_{r \in \mathcal{B}} r.c^2$ . To predict batch time, we sum the costs of non-attention operators and the attention costs, using either prefill- or decode-attention based on the request phase. For hybrid batches, both prefill- and decode-attention costs are added.

The figures demonstrate that linear models effectively capture operator costs. For non-attention operators, their times are linear to

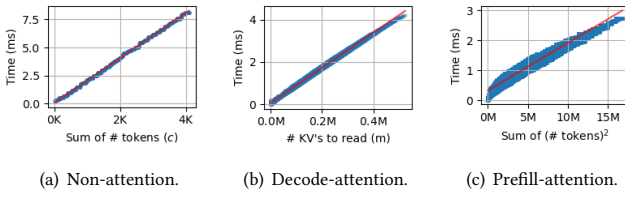


Figure 3: GPU times measured for a layer of the Llama-2-7B model on a A100 GPU [1]. Red lines are linear models with  $R^2$  scores of 0.999, 0.997, and 0.961.

the number of input tokens as they process tokens independently (Section 2.1). For example, given two matrices of size  $(c, h)$  and  $(h, H)$  where  $(c, h)$  represents input vectors with  $c$  input tokens and  $(h, H)$  represents model weights for input and output vector dimension of  $h$  and  $H$ , multiplying the two takes  $2chH$  arithmetic operations [54]. Therefore, it is linear to  $c$  as both  $h$  and  $H$  are fixed for a model. The decode-attention, being memory-bound, is bottlenecked by reading KVs from GPU memory, whose size is therefore linear to the number of KVs to read. The prefill-attention is compute-bound and exhibits quadratic complexity for computing the attention scores. In case of multiple GPUs where model weights are partitioned across GPUs, the amount of intermediate data to transfer between GPUs (outputs of matrix multiplications) also depends on the number of tokens to process [1], whose cost is also linear. We include it to the non-attention time for multiple GPUs. Biases capture additional fixed costs such as loading model weights. While changing hardware (GPU bandwidth and FLOPs), model (vector dimensions for non-attention operators and KV), or attention implementation [10, 11, 40] can affect these linear coefficients and biases, we fix those factors per experiment and make the batch time mainly depend on the number of input tokens and KVs read.

We further analyze the variance in Figure 3(c) that it is due to 1) chunked prefill and 2) kernel overhead. For 1), as the number of tokens processed  $m$  may not be zero, the complexity of attention is  $O((m + 1) + (m + 2) + \dots + (m + c)) = O(c^2 + 2mc)$ . Hence, we use  $\sum c^2 + 2mc$  instead of the  $\sum c^2$  from Figure 3(c). We also add a linear term of  $\sum m$  for reading KVs as decode-attention. For 2), we observe that the cost increases linearly to the number of prefill requests when using the standard attention implementation in [10, 11]. While a single GPU kernel processes all prefill requests, the number of launched thread blocks is linear to the number of prefill requests, where the GPU has a maximum number of thread blocks to run simultaneously. Executing multiple runs introduces a linear term. To learn the coefficients of these new terms, we calibrate the model to minimize the errors to actual GPU performance as in ⑤ in Figure 2. Overall, these reduce the relative error bound from more than 30% to 12%, with average relative error of 5.5% (Section 4.7).

We note that keeping cost models simple as linear enables light-weight estimation and embedding them in a higher-level problem, such as our CSP in Section 5 for finding the best assignment of requests to batches. These are yet effective enough to capture the relative performance of schedulers and develop a better one in the following sections.

Table 1: Schedulers used in the analysis. Each scheduler also has an eviction-free (EF) variant knowing the requests’ maximum memory usages.

Scheduler	Priority	Hybrid Batch	Chunked Prefill	$P$
vLLM	Prefill	X	X	4096
SARATHI	Decode	O	O	512
SARATHI <sub>P=C</sub>	Decode	O	O	4096
SARATHI <sub>nocp</sub>	Decode	O	X	4096
vLLM <sub>hy</sub>	Prefill	O	X	4096
SARATHI <sub>nohy</sub>	Decode	X	X	4096

With both schedulers and cost models in place, we can now simulate scheduler performance. Here, we primarily consider GPU time as the main overhead as in [1]. CPU overheads such as scheduling can be largely overlapped with GPU processing in more recent inference systems, as batches are scheduled asynchronously, leaving GPU computation as the critical path [54]. In databases, this is analogous to first focusing on query optimization performance in terms of execution time savings, rather than query optimizing time itself, which is out of our scope.

## 4 ANALYSIS

This section evaluates the performance of different schedulers using our framework and addresses key questions, some of which have received limited attention in previous studies.

### 4.1 Setup

**Model and Hardware.** We follow the default configuration of [1], using the Llama-2-7B model (whose  $C$  is 4096) on an A100 GPU with  $M = 100K$  as default. In Section 6, we scale up the model to 70B with  $C = 16384$  on four A100 GPUs to show that the insights found in this section generalize to other hardware-model configurations. We use 4 GPU hours to calibrate our cost models (⑤ in Figure 2).

**Schedulers.** Using [1] as a reference, we employ the vLLM [17] and SARATHI [2] schedulers as baselines. Table 1 lists the schedulers we compare, excluding certain variants that either performed similarly or worse in our experiments. We also implement eviction-free versions of the schedulers by reserving the maximum memory usage per request in the KV cache. In CANALLOCATE in Algorithm 1, we use  $m_{reserve} = I + O - 1$  for the request’s input and output length of  $I$  and  $O$ . Here,  $O$  includes the last EOS token that does not need to be processed. Since these schedulers assume that  $O$  is known in advance, they are hypothetical schedulers not deployable to real inference systems. Note that estimating  $O$  as in [37] is not our focus. While one can avoid evictions by using a known upper bound on memory usage, say  $C$ , this underutilizes memory and suffers from extremely low performance [17, 45].

**Workloads.** For clarity, we begin with fixed  $I$  and  $O$  across all requests, ranging from 1 to 1024 to cover a wide range of workloads where each request cannot be longer than  $C = 4096$ . This range is comprehensive enough, covering short-answer questions to long-text generations. For instance, a real-world workload [48] shows an average input length of 70 and output length of 215. We select request counts of  $B = 32$  and  $B = 1024$  to represent low and high contention scenarios. To simplify analysis, we use an offline setting where all requests arrive before scheduling begins, which can be

regarded as a snapshot of an online environment. In Section 6, we show that our insights generalize to online workloads with wider input and output ranges.

**Metrics.** We measure system performance using total latency and tokens-per-second (TPS), the number of generated tokens divided by latency. The time-to-first-token (TTFT) and time-per-output-token (TPOT) indicate the delay to generate the first token per request and the average interval to generate subsequent tokens [3, 17], which we use to evaluate request-level performance.

## 4.2 Under Low Contention

Under low contention ( $B = 32$ ), no evictions occur across all schedulers. We categorize the schedulers in Table 1 into 1) SARATHI<sub>nohy</sub>, 2) SARATHI, and 3) the others based on their performance. Figure 4 shows the results of representative schedulers.

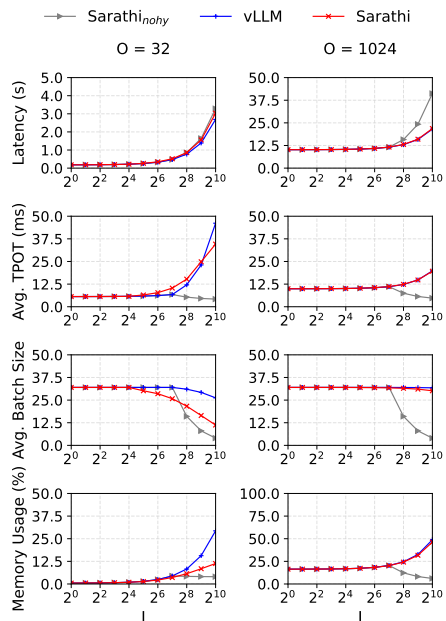


Figure 4: Results for small  $B$  of 32. Each column represents a specific  $O$ , with  $I$  on the x-axis.

The latency increases across all schedulers as  $I$  and  $O$  increase. vLLM consistently achieves the lowest latency by prioritizing pre-fills and batching as many decodes as possible, resulting in large batch sizes and reduced latency without evictions. Other schedulers in the same group with vLLM also have  $P = C = 4096$ , yielding similar prefill speeds and overall performance.

For  $O = 32$ , SARATHI experiences higher latency and TPOT than vLLM due to smaller batch sizes, as it processes only  $P = 512$  prefill tokens at a time, which reduces the number of decode requests and generated tokens in each batch. However, for  $O = 32$  and  $I = 1024$ , SARATHI achieves a lower TPOT than vLLM, as vLLM reads more KVs from the cache, resulting in heavier decode batches. For  $O = 1024$ , SARATHI shows similar performance with vLLM as the decode steps become prevalent.

SARATHI<sub>nohy</sub> exhibits a unique pattern, with high latency as  $I$  increases. This is due to a significant decrease in batch size for the following reasons. First, each prefill batch can add up to  $C/I$  requests, which decreases as  $I$  increases. Second, due to the disabled hybrid batching, if any running request is in the decode phase, it triggers a decode-only batch, whose size is limited by the first reason. Furthermore, these decode-only batches persist until all running requests complete.

**Remark.** Under low contention, evictions do not occur, and latency primarily depends on batch size, prefill speed, and the efficiency of batched decodes. vLLM achieves the fastest prefill speed by prioritizing pre-fills and processing up to  $C$  prefill tokens per batch. Larger batches can reduce TPOT, although an increase in the number of KVs to read may increase TPOT.

## 4.3 Under High Contention

We focus on the high-contention scenario with  $B = 1024$  to trigger evictions. We group the schedulers in Table 1 based on their performance into: 1) SARATHI, 2) SARATHI<sub>P=C</sub> and SARATHI<sub>nohy</sub>, and 3) vLLM and vLLM<sub>hy</sub>. We exclude SARATHI<sub>nohy</sub> due to its significantly higher latency and TTFT (Section 4.2). Figure 5 shows the results for SARATHI, SARATHI<sub>P=C</sub>, and vLLM as representatives.

Overall, as  $I$  and  $O$  increase, latency increases across all schedulers. As in Section 4.2, vLLM shows the lowest latency and highest TPS by prioritizing prefill requests and batch processing decodes in parallel, resulting in large batch sizes, except when high  $O$  values lead to frequent evictions. Eviction rates increase with  $O$  because each request competes to keep more tokens in the KV cache. SARATHI generally has the highest latency (up to 13.5% higher than vLLM) but achieves a stable TPOT (up to 5.3x lower than vLLM) due to balanced handling of prefill and decode phases through hybrid batching and a smaller  $P$  relative to  $C$ . SARATHI<sub>P=C</sub> strikes a middle ground, achieving nearly the highest TPS for each  $O$ , though it resembles vLLM more closely as it processes up to  $C$  prefill tokens per batch, matching vLLM's prefill speed by managing up to  $C/I$  new running requests per batch. Below, we discuss these trends in further detail.

**TPS.** TPS peaks as  $B$  increases, allowing more requests to process concurrently, generating more tokens per batch. However, TPS declines as  $I$  increases due to higher prefill costs. Beyond a certain point of  $O$ , TPS decreases because small  $O$  values make prefill dominant, while large  $O$  values make subsequent decode batches heavier, as decode costs scale linearly with the number of tokens or KVs read (Figure 6).

**TTFT and TPOT.** TTFT and TPOT reveal a trade-off, where TTFT reflects prefill time and TPOT reflects decode time in general. vLLM and SARATHI<sub>P=C</sub> achieve lower TTFT but higher TPOT than SARATHI. Schedulers other than SARATHI can process up to  $C$  prefill tokens per batch, starting pre-fills early, which minimizes TTFT but increases TPOT due to larger batch sizes and more KVs read in subsequent decode steps.

An interesting point is that TPOT decreases beyond a certain value of  $I$  (Figure 5). For large  $O$  (e.g., 1024), frequent evictions cause refills to dominate runtime, while larger  $I$  limits batch sizes and reduces evictions. This reduces time intervals between token generations. For small  $O$ , refills have a smaller impact, so TPOT

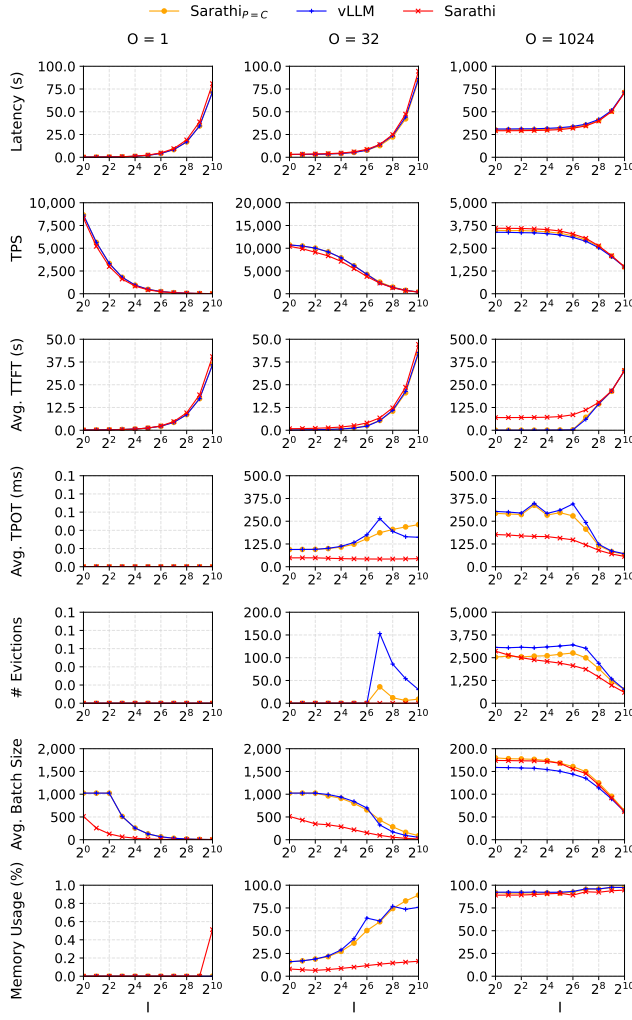


Figure 5: Results for large  $B$  of 1024.

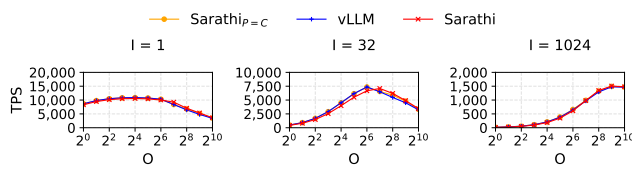


Figure 6: TPS for  $B$  = 1024.

more directly reflects batch size and the number of KVs read, as previously noted.

**Evictions and batch size.** The KV cache size  $M$  limits the maximum running requests in both prefill and decode phases, while the number of new running requests per batch is limited by prefill tokens  $P$ . Since at most  $P/I$  requests can be newly run per batch, large  $I$  decreases both batch size and the number of running requests, leading to fewer evictions as  $I$  increases (Figure 5). However,

$I$  and  $O$  also determine the memory reserved per request, so small values for  $I$  and  $O$  result in fewer evictions.

The key distinction between  $I$  and  $O$  in terms of their impact on evictions is that  $I$  represents the immediate memory reserved, whereas  $O$  determines the peak memory usage after approximately  $\Omega(O)$  batches have been processed. Consequently, schedulers that only consider  $I$  but not  $O$  risk overloading the system by batching requests with their long-term memory demands underestimated. As  $O$  increases, this can lead to a significant increase in the number of evictions.

**Memory (KV Cache) Usage.** For  $O = 1$ , only SARATHI shows a positive KV count at  $I = 1024$ , as it partitions  $I$  into smaller chunks with  $P = 512 < I$ , storing KVs for partially processed prompts in memory. Other schedulers complete requests in a single step by generating one EOS token and releasing the prompt.

Because SARATHI gradually adds running requests, it maintains stable memory consumption for KVs. However, for  $O = 1024$ , SARATHI experiences high memory demand, occupying more than 90% of the KV cache alike other schedulers.

**Remark.** Schedulers face a basic TTFT-TPOT trade-off. SARATHI maintains a balanced TTFT and TPOT across varying  $I$ ,  $O$ , and  $B$ . Other schedulers excel with moderate values but encounter eviction spikes under high memory demands due to aggressive batching. SARATHI mitigates this with a smaller  $P$  relative to  $C$ . High TPOT results primarily from evictions, with batch size and KV load as secondary factors. Evictions rise with larger  $B$  and  $O$  values, while  $I$  acts as both a limiting factor (as new running requests are bounded by  $P/I$ ) and an increasing factor (by raising memory demands). Testing on a live inference system (Section 4.7) confirms these trends.

#### 4.4 How Good Is It to Avoid Evictions?

With a basic understanding of the factors affecting performance, we can explore some key questions. Figure 7 provides a high-level roadmap for the upcoming sections. We begin by comparing the schedulers in Table 1 to their eviction-free versions. We use  $O = B = 1024$ , a scenario with frequent evictions, since in other cases, eviction-free (EF) schedulers perform similarly to their original (non-EF) counterparts.

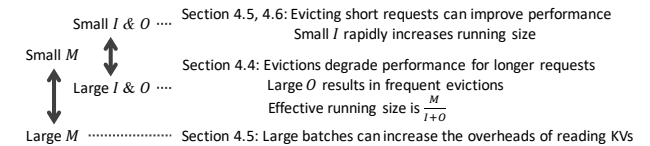
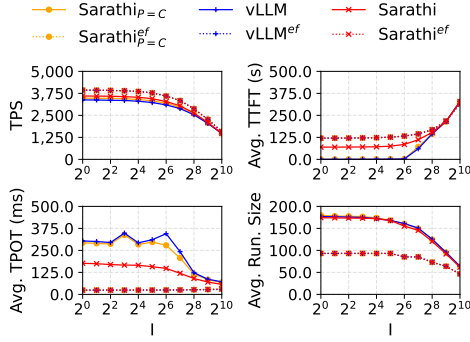


Figure 7: An overview of key insights in upcoming sections.

As illustrated in Figure 8, EF schedulers generally achieve better system performance, with TPS improvements over their non-EF versions reaching up to 17%, 9.6%, and 13.8% for vLLM, SARATHI, and SARATHI<sub>P=C</sub>. However, EF schedulers exhibit higher TTFT since they try to reserve more memory in initiating requests, waiting more for the current running requests to complete and release their KVs. This TTFT increase is substantial – up to 1000x for vLLM and SARATHI<sub>P=C</sub>, and 1.7x for SARATHI – but is offset by lower



**Figure 8: Results for  $O = B = 1024$ . Eviction-free (EF) schedulers are indicated by the  $ef$  superscript in the labels.**

TPOT, with reductions of up to 13x for vLLM and  $SARATHI_{P=C}$ , and 7.4x for  $SARATHI$ . Thus, the general TTFT-TPOT trade-off remains consistent even for EF schedulers.

**Remark.** Based on the results from the previous section, it is crucial to limit the number of running requests by considering  $M$  and the memory demands of requests. The *effective* running size can be approximated as  $\frac{M}{I+O}$ , as supported by Figure 8, where EF schedulers achieve an average running size close to  $\frac{100K}{I+1024} \approx 98$  and  $\frac{100K}{1024+1024} \approx 49$ .

#### 4.5 Is Increasing $M$ a Silver Bullet?

To avoid evictions and maximize the effective running size, one might wonder if simply increasing  $M$  to a sufficiently large value could solve all issues, possibly with multiple or state-of-the-art GPUs. To explore this, we vary  $M$  from 100 to 1M, testing under different memory contention levels and hardware-model configurations to simulate lower memory budgets. Figure 9 shows results for  $O = 32$  and  $B = 1024$ .

Interestingly, when  $M$  is small, EF schedulers actually show lower TPS compared to non-EF ones, as they wait too long for running requests to release memory. In this context, evictions can surprisingly boost TPS and reduce latency, a phenomenon we further prove in Section 5.1. As seen in Figure 9, evictions increase TPS by up to 1.9x and 2x for vLLM and  $SARATHI$ , with  $M = 100$ , and by 1.3x and 1.1x with  $M = 1K$ , mainly due to reduced TTFT, similar to the trends observed between vLLM and  $SARATHI$  in previous sections. However, these gains come with higher TPOT as a trade-off.

We emphasize that these results align with the results on a real inference system (Section 4.7), where evictions yield similar TPS increases up to 2.3x for  $M = 100$  and 1.4x for  $M = 1K$ . However for larger  $M$  values, evictions rather reduce TPS by up to 1.5x for  $M = 10K$  and 1.2x for  $M = 100K$ .

For small  $M$  in Figure 9, e.g.,  $M = 1K$ , vLLM shows lower TPS than  $SARATHI$  when  $I$  is small, since the rapid increase in running size leads to frequent evictions. However, vLLM surpasses  $SARATHI$  once  $M$  reaches a sufficiently large size.

An intriguing effect occurs with large  $M$  values, like 100K and 1M: TPOT for vLLM increases as  $M$  and  $I$  increase. For vLLM, approximately  $M/I$  running requests accumulate to fill the KV

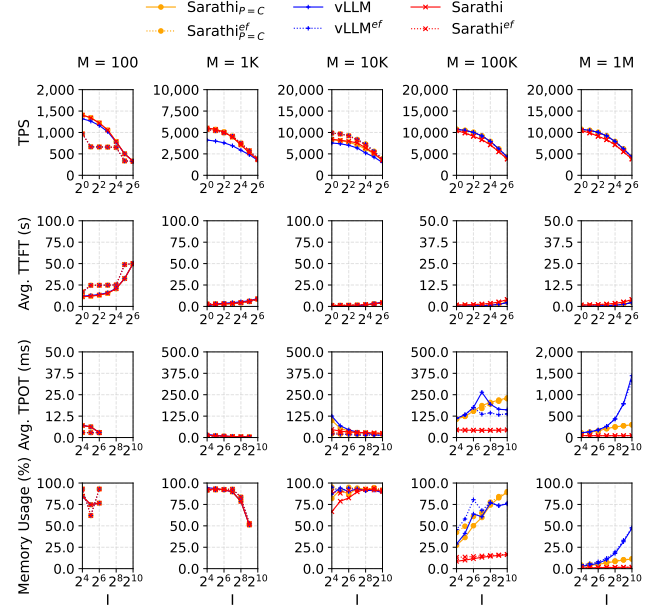


**Figure 9: Results for  $O = 32$  and  $B = 1024$  with varying  $M$ . The x-axes are cropped to display only the areas of interest.**

cache. Thus, the initial decode batch has a size of  $M/I$ , requiring  $M$  KVs to be read, which imposes a heavy load on the decode steps as  $M$  increases. With larger  $I$ , the waiting time for other prefill requests to complete also increases. Before the first decode batch, the system processes about  $M/P$  prefill batches, each taking  $O(P \cdot I)$  time, due to  $P/I$  requests per batch and the quadratic complexity  $O(I^2)$  of prefill operations. As a result, the total prefill time is  $O(M/P \cdot P \cdot I) = O(M \cdot I)$ . With sufficiently large  $M$ , evictions are minimized even for small  $I$ , causing each decode batch to quickly add  $M/I$  KVs to memory (due to  $M/I$  running requests), which, for smaller  $M$ , would instead lead to frequent evictions and also increase TPOT.

**Remark.** The results in this section highlight that increasing  $M$  alone is not a complete solution. Enhanced memory bandwidth is also essential to minimize the cost of reading KVs, as this factor contributes to the linear term in the decode cost model (Section 3.2). Additionally, Figure 9 shows that even with  $M = 1M$ ,  $SARATHI$  and  $SARATHI_{P=C}$  utilize less than 20% of  $M$  on average, even when processing numerous long requests, highlighting potential under-utilization.

#### 4.6 How Should We Prioritize Requests with Different Lengths?

Until now, we have assumed uniform input and output sizes for all requests. In the case of heterogeneous requests, prioritizing those with fewer steps, i.e., smaller output sizes, is known to improve scheduling efficiency [13, 37, 50]. However, we question this approach, finding that input size can be an equally or more important factor.

We compare three ranking-based schedulers that prioritize requests by short input or output sizes rather than by phase (prefill or decode). These schedulers can be implemented by grouping and ordering requests by input or output size in `GROUPREQUESTS` in Algorithm 1.

- $Rank_{org}$ : No prioritization by  $I$  or  $O$ .
- $Rank_I$ : Prioritize requests with small  $I$ .
- $Rank_O$ : Prioritize requests with small  $O$  (thus hypothetical).

Regarding the workloads, we generate each workload as a mix of two groups from the following four groups (with  $S = \{8, 16\}$ ,  $L = \{512, 1024\}$ ):

- Small  $I$  and Small  $O$  (SISO):  $I \in S, O \in S$
- Small  $I$  and Large  $O$  (SILO):  $I \in S, O \in L$
- Large  $I$  and Small  $O$  (LISO):  $I \in L, O \in S$
- Large  $I$  and Large  $O$  (LILO):  $I \in L, O \in L$

The requests in each workload are randomly shuffled, and the number of requests  $B$  varies from 16 to 1024.

**Latency.** Figure 10 shows the latencies for six workloads with different query group mixes. Prioritizing requests with smaller  $I$  can reduce latency. When the KV cache reaches  $M$  and frequent evictions occur as  $B$  increases, scheduling smaller  $I$  requests first, despite evictions and refills, can reduce latency. Consequently,  $Rank_I$  shows up to 1.3x lower latency than  $Rank_O$  and  $Rank_{org}$ , particularly in the LILO+SISO workload (top middle in Figure 10) with frequent evictions.

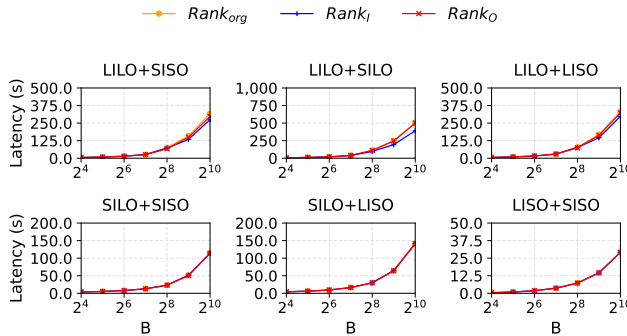


Figure 10: Latency over heterogeneous workloads.

**TTFT.** Scheduling requests with small  $I$  or  $O$  first can reduce TTFT by prioritizing short-running requests. For example, assume two requests  $R1$  and  $R2$  with different  $I$  values, where their (prefill time, decode time) pairs are  $(1, 1)$  and  $(2, 1)$ . Scheduling  $R1$  first yields an average TTFT of  $(1 + (1 + 1 + 2))/2 = 5/2$ , while scheduling  $R2$  first results in  $(2 + (2 + 1 + 1))/2 = 6/2$ . If the (prefill time, decode time) pairs are  $(1, 1)$  and  $(1, 2)$ , then scheduling  $R1$  first results in the average TTFT of  $(1 + (1 + 1 + 1))/2 = 4/2$ , where scheduling  $R2$  first results in  $(1 + (1 + 2 + 1))/2 = 5/2$ . As Figure 11 shows,  $Rank_I$  achieves up to 3.1x and 2.3x lower TTFT than  $Rank_O$  and  $Rank_{org}$  for all workloads except LILO+LISO, where requests have similar  $I$ .

**TPOT.** Prioritizing requests with small  $I$  or  $O$  can lower TPOT by minimizing evictions or avoiding heavy batches. Assume that we process long requests with large  $I$  and short requests with small  $I$  together where long requests are scheduled first. If the memory is

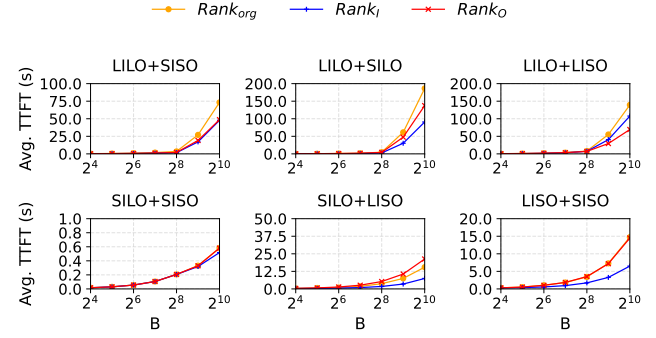


Figure 11: Average TTFT over heterogeneous workloads.

limited (e.g., in workloads containing LILO) and evictions occur for the short requests, they need to wait longer for long requests to release their memory. Therefore, prioritizing short requests leads to a comparatively lower waiting time. This is why in Figure 12  $Rank_I$  has up to 1.4x smaller TPOT than  $Rank_O$  and  $Rank_{org}$ , on the workloads that contain LILO and evictions occur frequently.

However, prioritizing small  $I$  may also increase TPOT as the batch size increases, where  $P/I$  requests can be added to the running requests per batch.  $Rank_O$  shows up to 3.9x and 1.8x smaller TPOT than  $Rank_I$  and  $Rank_{org}$  on the workloads that do not contain LILO and having fewer evictions.

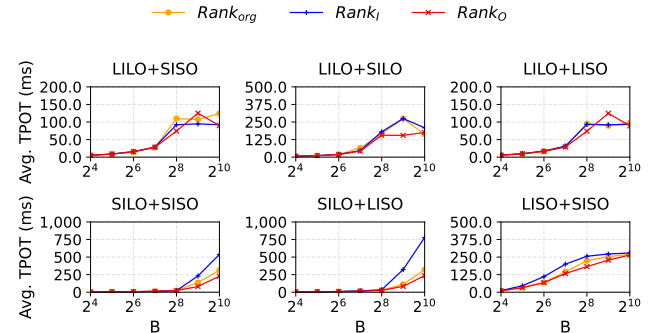


Figure 12: Average TPOT over heterogeneous workloads.

**Remark.** Prioritizing requests with smaller  $I$  generally yields better performance compared to prioritizing smaller  $O$ , except when (1) requests have similar  $I$  but highly variable  $O$ , or (2) memory is sufficient (thus fewer evictions) as in workloads without LILO, with TPOT being a critical metric (batch size should be kept small). In such cases, prioritizing smaller  $O$  is more effective. These are notable since most request-ranking studies have focused on output size [13, 37, 50]. We suggest that input size may be an equally or more significant factor.

## 4.7 Results on a Real Inference System

This section presents results from running the experiments in Sections 4.3 and 4.5 on a real inference system (Figures 13 and 14). We

use vLLM [17] v0.6.3. For clarity, vLLM refers to the scheduler as before, while vLLM-Sys denotes the inference system.

Figure 13 shows similar results with Figure 5, with the average and maximum relative error of 5.5% and 12% for latency. Non-GPU time mainly consists of CPU-based scheduling and token sampling, where we leave optimizing them as an orthogonal future work. Recent inference systems and techniques, e.g., asynchronous scheduling [54] mentioned in Section 3, allow effective overlapping of non-GPU and GPU operations.

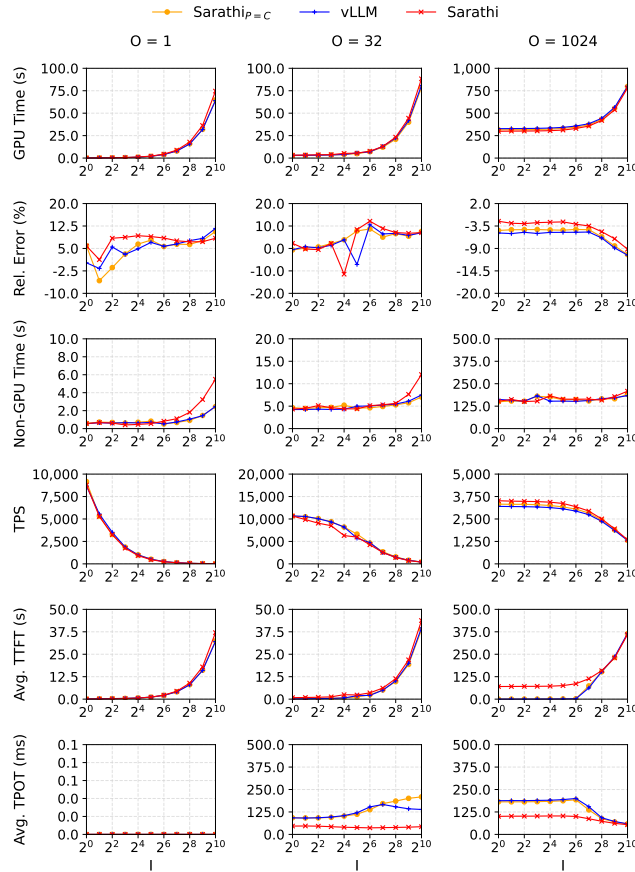


**Figure 13: Results of running the schedulers in Figure 5 on vLLM-Sys with  $B = 1024$ . GPU time represents the duration for GPU-based operations, including matrix multiplications and attentions, while non-GPU time covers scheduling and token sampling. The second row indicates the relative error of the latency in Figure 5 compared to the GPU time. TPS, TTFT, and TPOT are calculated using GPU times only.**

Figure 14 shows results for varying  $M$ . Consistent with Section 4.5, evictions increase TPS up to 2.3x for small  $M$  values of 100 and 1K, but decrease TPS up to 1.5x for larger  $M$  values.

## 5 OPTIMAL SCHEDULING AS CONSTRAINT SATISFACTION PROBLEM

This section applies constraint satisfaction problem (CSP) [39] to find optimal schedules and prove the insights found in previous

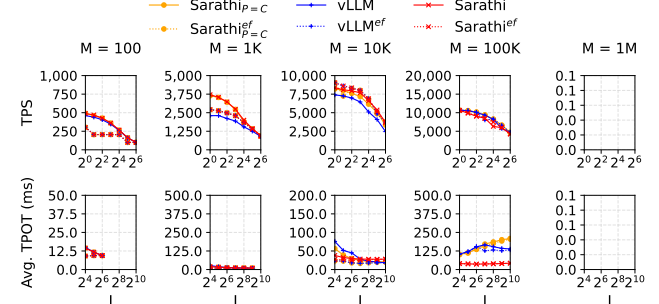


**Figure 14: Results of running the schedulers in Figure 9 on vLLM-Sys with  $O = 32$  and  $B = 1024$ . No results are provided for  $M = 1M$  since the maximum  $M$  available on the physical A100 GPU with the Llama-2-7B model is below 1M.**

analysis. To the best of our knowledge, this is the first attempt to apply CSP to LLM inference scheduling. As CSP utilizes output lengths of requests, it is hypothetical. Unlike other schedulers that specify *how* to schedule requests algorithmically, solving CSP gives *what*: one or more schedules that 1) satisfy constraints specifying scheduling policies and 2) achieve the best performance objectives, as well as the achievable performance bounds.

Performance upper bounds allow for a more goal-oriented development of efficient inference techniques, determining promising ideas that are worth developing, unlike naively seeking a better scheduling algorithm without assured performance improvements. For instance, we can validate whether a better schedule exists that could reduce the latency of current schedules by 10% for specific workloads. The optimization target can be adjusted to meet objectives such as latency, throughput, or fairness, if these can be represented in a formula.

In our CSP formulation, we first establish key notations. The index  $i \geq 1$  and  $j \geq 1$  represent the  $i$ -th request  $r_i$  and  $j$ -th batch  $\mathcal{B}_j$ . We also use  $j = 0$  as a virtual index to denote the initial system state. Each  $r_i$  has an input size (number of prompt tokens)  $I_i$  and output size  $O_i$ . We use  $\mathbb{I}_c$  as the indicator variable, 1 if a condition  $c$  is true and 0 otherwise. Now we explain the three parts of our CSP: variables, constraints, and objectives.

**Variables.**  $S_{i,j}$  represents the number of all prompt and generated tokens for  $r_i$  after processing  $\mathcal{B}_j$ , with  $S_{i,0} = I_i$ .  $m_{i,j}$  denotes  $r_i.m$  after processing  $\mathcal{B}_j$ , with  $m_{i,0} = 0$ .  $c_{i,j}$  denotes  $r_i.c$  at  $\mathcal{B}_j$ , which can be 0 if  $r_i \notin \mathcal{B}_j$ .  $g_{i,j} = \mathbb{I}_{r_i \text{ generates a token at } \mathcal{B}_j}$  and  $e_{i,j} = \mathbb{I}_{r_i \text{ is evicted at } \mathcal{B}_j}$ .

**Constraints.** The constraints establish the interactions between variables and the conditions necessary for a valid schedule.

**Termination:**  $r_i$  must generate  $O_i$  tokens, thus  $\forall i : \sum_j g_{i,j} = O_i$ .

**Non-Decreasing Sequence Length:**  $\forall i, j : S_{i,j} = S_{i,j-1} + g_{i,j}$ .

**Memory Management:**  $m$  should be 0 if  $r_i$  is evicted or should increase by  $c_{i,j}$ .

$$\forall i, j : m_{i,j} = \begin{cases} 0 & \text{if } e_{i,j} = 1 \\ m_{i,j-1} + c_{i,j} & \text{otherwise} \end{cases} \quad (1)$$

Tokens to Process:  $c$  should be 0 if  $r_i$  is evicted or should not exceed available tokens to process.

$$\forall i, j : c_{i,j} = \begin{cases} 0 & \text{if } e_{i,j} = 1 \\ \leq S_{i,j-1} - m_{i,j-1} & \text{otherwise} \end{cases} \quad (2)$$

Token Generation:  $g$  can only be 1 if all tokens are processed, for both (chunked) prefill and decode steps.

$$\forall i, j : g_{i,j} = \begin{cases} 1 & \text{if } c_{i,j} = S_{i,j-1} - m_{i,j-1} \\ 0 & \text{otherwise} \end{cases} \quad (3)$$

Batch Constraints: Ensures global constraints per batch.

$$\forall j : \sum_i c_{i,j} \leq C, \sum_i m_{i,j} \leq M \quad (4)$$

For brevity, we omit other indicator variables representing whether a request is in prefill or decode phase and a constraint using  $P$  for chunked prefill. Still, the inequality in (2) allows partial processing of the available tokens as in chunked prefill.

For implementing conditional constraints (1)-(3), we use the Big-M method [35] to linearize them, since linear programs are more efficient than non-linear ones [7]. For example, (1) is linearized as:

$$\begin{aligned} m_{i,j} &\leq M(1 - e_{i,j}), \\ m_{i,j} &\leq m_{i,j-1} + c_{i,j} + M e_{i,j}, m_{i,j} \geq m_{i,j-1} + c_{i,j} - M e_{i,j}, \end{aligned} \quad (5)$$

where  $M$  is a sufficiently large constraint. We implement our CSP using GUROBI<sup>4</sup>.

One might wonder why there is no constraint for  $e_{i,j}$  and why we need to define such a variable when finding optimal schedules. First, even without such a constraint, (4) can force  $e_{i,j}$  to be nonzero to retain memory. Second, we have seen in Section 4 that evictions can improve performance compared to waiting for other requests to finish, which we prove shortly.

**Objective.** The objective can be set to minimize total latency using our cost models in Section 3.2, summing up all batch times. Instead of retrieving the minimum latency, one can simply opt for the existence of a better schedule, for example, by running a scheduler whose latency is  $L$  and adding a constraint that the latency should be less than  $0.9L$  to guarantee 10% improvement.

**Online Setting.** Supporting an online setting, where each request  $r_i$  has an arrival time  $T_i$ , is straightforward: add a variable  $Acc_j$  to track accumulated batch times and set  $S_{i,j} = m_{i,j} = 0$  if  $Acc_j < T_i$ . **Challenge.** A primary challenge in CSP is its limited scalability, as it is generally NP-complete [38]. The complexity grows with the number of requests and batches, reaching millions of variables for thousands of requests and batches. Consequently, we primarily use CSP on small workloads that are enough to explain the phenomena found in Section 4 and initialize the variables with outputs from other schedulers, rather than using all-zero or random values. We leave optimizing CSP for larger scales as a future work with possibly approximation approaches [27, 29].

<sup>4</sup><https://www.gurobi.com>

## 5.1 Can Evictions Be Optimal?

As noted in Section 4.5, evictions can sometimes enhance system performance. We use our CSP as a proof-by-example approach. We set  $O = B = 4$  and vary  $I$  from 1 to 1024, with  $M = \max(2I, I+O-1)$ . This allows scheduler to initiate prefills for two requests ( $2I$ ) while ensuring that only one request can retain its KVs to generate the final token ( $I+O-1 \leq M < 2(I+O-1)$ ). The objective is to minimize latency.

Interestingly, the CSP also opts to evict requests, similar to non-EF schedulers. For  $I \leq 32$ , CSP chooses to evict short requests, as illustrated in Figure 15(a), because it is faster to begin generating tokens with short prefills and finish requests early albeit being evicted in later batches, rather than wait for enough memory to be released. This approach can reduce latency by up to 17% compared to EF schedules as  $I$  decreases. However, for  $I \geq 64$ , CSP avoids evictions, as the later refill cost grows quadratically with prompt size. Here, avoiding evictions can reduce latency by up to 40% as  $I$  increases. Among the schedulers, vLLM and its EF version exhibit latency results close CSP’s results, for  $I \leq 32$  and  $I \geq 64$ , respectively.

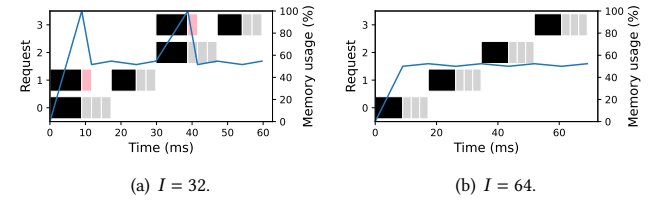


**Figure 15: CSP results for  $O = B = 4$  and  $M = \max(2I, I+O-1)$ .** Black, gray, and red boxes indicate requests in the (p)refill, decode, and evict phases, respectively. Blue lines represent memory (KV cache) usage over time.

**Remark.** While it is counterintuitive that evictions improve performance, we prove that it is true and find a relationship between sequence length and performance improvement by evictions. Evicting short requests can help, but evicting long requests degrades performance due to high refill costs. Furthermore, note in Figure 15 that  $M$  is underutilized as in Figure 9, leaving an additional room for improvement.

## 6 HARNESSING EVICTIONS IN SCHEDULING

We translate our insights obtained in previous sections into a deployable scheduler. In Algorithm 1, we group requests into  $\mathcal{R}_r^d$ ,  $\mathcal{R}_r^p$ , and  $\mathcal{R}_w$  as in SARATHI, prioritizing running requests. For  $\mathcal{R}_r^d$ , we further prioritize running *long* requests (having larger  $m$ ) and evict *short* requests if memory is insufficient. This is to avoid large refill costs after evicting long requests. Note that this is different from both  $Rank_I$  and  $Rank_O$  schedulers in Section 4.6 as we rather prioritize long requests. By adding a single line of this **sorting**, which is extremely easy to implement, we show that it can incur substantial GPU savings. We further maintain an online **histogram** to estimate the output lengths of requests and reserve the estimated maximum memory usage in **3** of Algorithm 1.

We test our scheduler on a real-world workload with 1 hour trace of conversations from multiple users [5]. It contains 19.7K LLM requests where the average and maximum input sizes are 1.2K and 14.1K, and the average and maximum output sizes are 0.2K and 1K. We use Llama-3-70B model with  $C = 16384$  on four A100 GPUs, and  $M = 100K$  as before.

Figure 16 shows the results on the real inference system vLLM-Sys (Section 4.7), where only the runtime of the leftmost method is estimated as it is not runnable (estimation error is 2 to 5% for other methods). We use it as an performance upper bound assuming indefinite resource. Surprisingly, our simple ideas solve half of the problem, reducing 7K seconds of deployable schedulers to 6K seconds, where the performance bound is 5K seconds. Ours also outperform EF schedulers without any evictions.

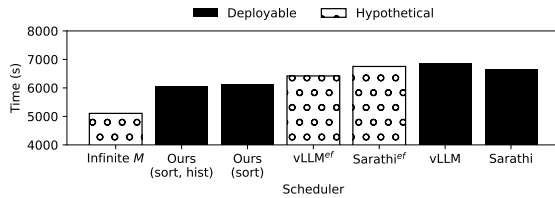


**Figure 16: Results on vLLM-Sys using a real-world workload [5] and four A100 GPUs. The leftmost method is estimated by our cost models and vLLM scheduler with indefinite  $M$ .**

## 7 RELATED WORK

**LLM Inference System.** ORCA [45] introduces continuous batching, vLLM [17] proposes paged attention, and SARATHI [2, 3] implements hybrid batching and chunked prefill. Instead of hybrid batching, DISTSERVE [52] and DEJAVU [41] disaggregate prefill and decode phases by using different GPUs, sending the KV cache from the prefill- to decode-handling GPU. vTENSOR [44] decouples the KV cache allocation and attention computation in vLLM, removing the page address translation overhead. INFINIGEN [18] offloads the KVs to CPU memory to extend the KV cache and reloads the KVs from CPU layer-wise. To minimize the data transfer overhead, it streams only the KVs of the most important tokens and approximates the full attention result. NANOFLOW [54] proposes nano-batching that further partitions each batch to overlap intra-layer operators. INSTINFER [32] uses flash drives to offload KVs and attention computations. We employ the standard techniques in ORCA, vLLM, and SARATHI in this study. Other systems focus on hardware-specific optimizations but less on request scheduling. Still, we envision that our cost modeling, CSP formulation, and cost-effective development approach can be applied to those systems with extended cost models and scheduling-like policies to optimize.

**LLM Inference Simulation.** Our work extends VIDUR [1], which proposes simulation of LLM inference for the first time. It allows LLM service providers to predict the best system and hardware configuration under a budget. However, it focuses on searching configurations, but lacks an in-depth analysis or new insights for developing better schedulers given an environment, as well as our hypothetical schedulers including CSP to predict performance upper bounds.

**Output Length Prediction.** Several studies aim to estimate or rank the output lengths of requests to improve scheduling efficiency [13, 37, 50]. While such an estimation is out of our scope, our approach complements these work by examining the fundamental question of how much improvement they can offer, using our hypothetical schedulers leveraging the exact output lengths. This is analogous to assessing the performance bound of the impact of cardinality estimation on query plans by leveraging exact cardinalities, before applying yet another estimator [19]. Furthermore, our findings also apply to scenarios where requests have identical lengths.

## 8 FUTURE WORK

This section explains several research problems in more complex systems, hardware, and workloads as future work. First, to develop more effective scheduling policies and cost models, reinforcement learning could be used to generate and refine candidate policies and models against estimated or real costs, while comparing with scaled CSP solutions to bridge any gaps in performance, reducing the need for manual optimization.

Building on our work, we further envision modeling costs and scheduling policies on different storage hierarchies and inference systems with more complex data management policies such as KV offloading to CPUs and storage [18, 32]. With simulation-based analysis on diverse workloads and proofs via CSP, this would lead to more cost-efficient development cycles and efficient inference systems, with potential reductions in operating costs.

Hardware and model characteristics determine resource constraints like  $M$  and  $C$  as well as cost model coefficients and biases (Section 3.2). Future work could explore new hardware capabilities, prefill-decode disaggregation [34, 41, 52] hardware acceleration [22], model quantization [12, 26], KV compression [24], attention techniques optimized for reduced data loads with a trade-off of losing information [6, 14, 15], and speculative decoding and model cascades that selectively use smaller to larger models based on task complexity [20, 33].

Expanding to more complex scenarios beyond offline and online workloads will also be crucial as inference patterns grow in complexity, including prefix sharing between requests, connecting multiple requests via input-output relationships, multi-path reasoning, and compound AI systems that connect LLMs to other data processing components such as document retrieval and SQL calls [16, 23, 33, 47, 49, 51]. Therefore, exploring these will have significant impact on database applications and systems using LLMs.

## 9 CONCLUSION

In this work, we tackle a data management issue in LLM inference from its ever-increasing demands in daily tasks and database applications. We provide an analytical framework to compare schedulers and benchmark them against optimal and hypothetical scheduling policies for multiple concurrent queries. By incorporating the constraint satisfaction problem on top of our linear cost models, our approach theoretically proves scheduling inefficiencies. We propose simple, easy-to-implement scheduling policies to enhance the performance of LLM inference systems, which can lead to substantial GPU savings.

## REFERENCES

[1] Amey Agrawal, Nitin Kedia, Jayashree Mohan, Ashish Panwar, Nipun Kwatra, Bhargav S. Gulavani, Ramachandran Ramjee, and Alexey Tumanov. 2024. VIDUR: A Large-Scale Simulation Framework for LLM Inference. In *Proceedings of the Seventh Annual Conference on Machine Learning and Systems, MLSys 2024, Santa Clara, CA, USA, May 13-16, 2024*, Philip B. Gibbons, Gennady Pekhimenko, and Christopher De Sa (Eds.). mlsys.org.

[2] Amey Agrawal, Nitin Kedia, Ashish Panwar, Jayashree Mohan, Nipun Kwatra, Bhargav S. Gulavani, Alexey Tumanov, and Ramachandran Ramjee. 2024. Taming Throughput-Latency Tradeoff in LLM Inference with Sarathi-Serve. In *18th USENIX Symposium on Operating Systems Design and Implementation, OSDI 2024, Santa Clara, CA, USA, July 10-12, 2024*, Ada Gavrilovska and Douglas B. Terry (Eds.). USENIX Association, 117–134.

[3] Amey Agrawal, Ashish Panwar, Jayashree Mohan, Nipun Kwatra, Bhargav S. Gulavani, and Ramachandran Ramjee. 2023. SARATHI: Efficient LLM Inference by Piggybacking Decodes with Chunked Prefills. *CoRR* abs/2308.16369 (2023). <https://doi.org/10.48550/ARXIV.2308.16369> arXiv:2308.16369

[4] Peter Akiyama, Zixuan Yi, and Ryan Marcus. 2024. The Unreasonable Effectiveness of LLMs for Query Optimization. *arXiv preprint arXiv:2411.02862* (2024).

[5] Microsoft Azure. [n.d.]. Azure Public Dataset. <https://github.com/Azure/AzurePublicDataset>.

[6] Iz Beltagy, Matthew E. Peters, and Arman Cohan. 2020. Longformer: The Long-Document Transformer. *CoRR* abs/2004.05150 (2020). arXiv:2004.05150 <https://arxiv.org/abs/2004.05150>

[7] Dimitri Bertsimas and John N. Tsitsiklis. 1997. *Introduction to linear optimization*. Athena scientific optimization and computation series, Vol. 6. Athena Scientific.

[8] code4DB. 2024. LLM4DB: A Curated List of Resources on Large Language Models for Databases. <https://github.com/code4DB/LLM4DB>. Accessed: 2024-11-30.

[9] Zihang Dai, Zhilin Yang, Yiming Yang, Jaime G. Carbonell, Quoc Viet Le, and Ruslan Salakhutdinov. 2019. Transformer-XL: Attentive Language Models beyond a Fixed-Length Context. In *Proceedings of the 57th Conference of the Association for Computational Linguistics, ACL 2019, Florence, Italy, July 28–August 2, 2019, Volume 1: Long Papers*, Anna Korhonen, David R. Traum, and Lluís Márquez (Eds.). Association for Computational Linguistics, 2978–2988. <https://doi.org/10.18653/V1/P19-1285>

[10] Tri Dao. 2024. FlashAttention-2: Faster Attention with Better Parallelism and Work Partitioning. In *The Twelfth International Conference on Learning Representations, ICLR 2024, Vienna, Austria, May 7-11, 2024*. OpenReview.net. <https://openreview.net/forum?id=mZn2Xyh9Ec>

[11] Tri Dao, Daniel Y. Fu, Stefano Ermon, Atri Rudra, and Christopher Ré. 2022. FlashAttention: Fast and Memory-Efficient Exact Attention with IO-Awareness. In *Advances in Neural Information Processing Systems 35: Annual Conference on Neural Information Processing Systems 2022, NeurIPS 2022, New Orleans, LA, USA, November 28 - December 9, 2022*, Sammi Koyejo, S. Mohamed, A. Agarwal, Danielle Belgrave, K. Cho, and A. Oh (Eds.).

[12] Tim Dettmers, Mike Lewis, Younes Belkada, and Luke Zettlemoyer. 2022. GPT3.int8(): 8-bit Matrix Multiplication for Transformers at Scale. In *Advances in Neural Information Processing Systems 35: Annual Conference on Neural Information Processing Systems 2022, NeurIPS 2022, New Orleans, LA, USA, November 28 - December 9, 2022*, Sammi Koyejo, S. Mohamed, A. Agarwal, Danielle Belgrave, K. Cho, and A. Oh (Eds.).

[13] Yichao Fu, Siqi Zhu, Runlong Su, Aurick Qiao, Ion Stoica, and Hao Zhang. 2024. Efficient LLM Scheduling by Learning to Rank. *CoRR* abs/2408.15792 (2024). <https://doi.org/10.48550/ARXIV.2408.15792> arXiv:2408.15792

[14] Albert Gu, Karan Goel, and Christopher Ré. 2022. Efficiently Modeling Long Sequences with Structured State Spaces. In *The Tenth International Conference on Learning Representations, ICLR 2022, Virtual Event, April 25-29, 2022*. OpenReview.net.

[15] Edward J. Hu, Yelong Shen, Phillip Wallis, Zeyuan Allen-Zhu, Yuanzhi Li, Shean Wang, Lu Wang, and Weizhi Chen. 2022. LoRA: Low-Rank Adaptation of Large Language Models. In *The Tenth International Conference on Learning Representations, ICLR 2022, Virtual Event, April 25-29, 2022*. OpenReview.net. <https://openreview.net/forum?id=nZvEKKeeFyf9>

[16] Soyeong Jeong, Jinheon Baek, Sukmin Cho, Sung Ju Hwang, and Jong Park. 2024. Adaptive-RAG: Learning to Adapt Retrieval-Augmented Large Language Models through Question Complexity. In *Proceedings of the 2024 Conference of the North American Chapter of the Association for Computational Linguistics: Human Language Technologies (Volume 1: Long Papers)*, NAACL 2024, Mexico City, Mexico, June 16-21, 2024, Kevin Duh, Helena Gómez-Adorno, and Steven Bethard (Eds.). Association for Computational Linguistics, 7036–7050. <https://doi.org/10.18653/V1/2024.NAACL-LONG.389>

[17] Woosuk Kwon, Zhuohan Li, Siyuan Zhuang, Ying Sheng, Lianmin Zheng, Cody Hao Yu, Joseph Gonzalez, Hao Zhang, and Ion Stoica. 2023. Efficient Memory Management for Large Language Model Serving with PagedAttention. In *Proceedings of the 29th Symposium on Operating Systems Principles, SOSP 2023, Koblenz, Germany, October 23-26, 2023*, Jason Flinn, Margo I. Seltzer, Peter Druschel, Antoine Kaufmann, and Jonathan Mace (Eds.). ACM, 611–626. <https://doi.org/10.1145/3600006.3613165>

[18] Wonbeom Lee, Jungi Lee, Junghwan Seo, and Jaewoong Sim. 2024. InfiniGen: Efficient Generative Inference of Large Language Models with Dynamic KV Cache Management. In *18th USENIX Symposium on Operating Systems Design and Implementation, OSDI 2024, Santa Clara, CA, USA, July 10-12, 2024*, Ada Gavrilovska and Douglas B. Terry (Eds.). USENIX Association, 155–172.

[19] Viktor Leis, Andrei Gubichev, Atanas Mirchev, Peter Boncz, Alfons Kemper, and Thomas Neumann. 2015. How good are query optimizers, really? *Proceedings of the VLDB Endowment* 9, 3 (2015), 204–215.

[20] Yaniv Leviathan, Matan Kalman, and Yossi Matias. 2023. Fast Inference from Transformers via Speculative Decoding. In *International Conference on Machine Learning, ICML 2023, 23-29 July 2023, Honolulu, Hawaii, USA (Proceedings of Machine Learning Research)*, Andreas Krause, Emma Brunskill, Kyunghyun Cho, Barbara Engelhardt, Sivan Sabato, and Jonathan Scarlett (Eds.), Vol. 202. PMLR, 19274–19286. <https://proceedings.mlr.press/v202/leviathan23a.html>

[21] Zhaodonghui Li, Haitao Yuan, Huiming Wang, Gao Cong, and Lidong Bing. 2024. LLM-R2: A Large Language Model Enhanced Rule-based Rewrite System for Boosting Query Efficiency. *CoRR* abs/2404.12872 (2024). <https://doi.org/10.48550/ARXIV.2404.12872> arXiv:2404.12872

[22] Sean Lie. 2024. Inside the Cerebras Wafer-Scale Cluster. *IEEE Micro* 44, 3 (2024), 49–57. <https://doi.org/10.1109/MM.2024.3386628>

[23] Chaofan Lin, Zhenhua Han, Chengruidong Zhang, Yuqing Yang, Fan Yang, Chen Chen, and Lili Qiu. 2024. Parrot: Efficient Serving of LLM-based Applications with Semantic Variable. In *18th USENIX Symposium on Operating Systems Design and Implementation, OSDI 2024, Santa Clara, CA, USA, July 10-12, 2024*, Ada Gavrilovska and Douglas B. Terry (Eds.). USENIX Association, 929–945.

[24] Yuhan Liu, Hanchen Li, Yihua Cheng, Siddharth Ray, Yuyang Huang, Qizheng Zhang, Kuntai Du, Jiayi Yao, Shan Lu, Ganesh Ananthanarayanan, Michael Maire, Henry Hoffmann, Ari Holtzman, and Junchen Jiang. 2024. CacheGen: KV Cache Compression and Streaming for Fast Large Language Model Serving. In *Proceedings of the ACM SIGCOMM 2024 Conference, ACM SIGCOMM 2024, Sydney, NSW, Australia, August 4-8, 2024*. ACM, 38–56. <https://doi.org/10.1145/3651890.3672274>

[25] Alexandra Sasha Luccioni, Sylvain Viguier, and Anne-Laure Ligozat. 2023. Estimating the carbon footprint of bloom, a 176b parameter language model. *Journal of Machine Learning Research* 24, 253 (2023), 1–15. <https://www.jmlr.org/papers/volume24/23-0069/23-0069.pdf>

[26] Shuming Ma, Hongyu Wang, Lingxiao Ma, Lei Wang, Wenhui Wang, Shaohan Huang, Li Dong, Ruiping Wang, Jilong Xue, and Furu Wei. 2024. The Era of 1-bit LLMs: All Large Language Models are in 1.58 Bits. *CoRR* abs/2402.17764 (2024). <https://doi.org/10.48550/ARXIV.2402.17764> arXiv:2402.17764

[27] Konstantin Makarychev and Yury Makarychev. 2017. Approximation algorithms for CSPs.

[28] Xupeng Miao, Zhihao Jia, and Bin Cui. 2024. Demystifying Data Management for Large Language Models. In *Companion of the 2024 International Conference on Management of Data, SIGMOD/PODS 2024, Santiago AA, Chile, June 9-15, 2024*, Pablo Barceló, Natacha Sánchez-Pi, Alexandra Meliou, and S. Sudarshan (Eds.). ACM, 547–555. <https://doi.org/10.1145/3626246.3654683>

[29] Steven Minton, Mark D Johnston, Andrew B Philips, and Philip Laird. 1990. Solving large-scale constraint satisfaction and scheduling problems using a heuristic repair method. In *Proceedings of the eighth National conference on Artificial intelligence-Volume 1*. 17–24.

[30] ModelITC. 2023. LightLLM: A python-based large language model inference and serving framework. <https://github.com/ModelITC/lightllm>.

[31] NVIDIA. [n.d.]. Faster Transformer. <https://github.com/NVIDIA/FasterTransformer>.

[32] Xiurui Pan, Endian Li, Qiao Li, Shengwen Liang, Yizhou Shan, Ke Zhou, Yingwei Luo, Xiaolin Wang, and Jie Zhang. 2024. InstInfer: In-Storage Attention Offloading for Cost-Effective Long-Context LLM Inference. *CoRR* abs/2409.04992 (2024). <https://doi.org/10.48550/ARXIV.2409.04992> arXiv:2409.04992

[33] Liana Patel, Siddharth Jha, Carlos Guestrin, and Matei Zaharia. 2024. LOTUS: Enabling Semantic Queries with LLMs Over Tables of Unstructured and Structured Data. *CoRR* abs/2407.11418 (2024). <https://doi.org/10.48550/ARXIV.2407.11418> arXiv:2407.11418

[34] Pratyush Patel, Esha Choukse, Chaojie Zhang, Aashaka Shah, Íñigo Goiri, Saeed Maleki, and Ricardo Bianchini. 2024. Splitwise: Efficient Generative LLM Inference Using Phase Splitting. In *51st ACM/IEEE Annual International Symposium on Computer Architecture, ISCA 2024, Buenos Aires, Argentina, June 29 - July 3, 2024*. IEEE, 118–132. <https://doi.org/10.1109/ISCA59077.2024.00019>

[35] Efstratios N. Pistikopoulos. 1998. C.A. Floudas, Nonlinear and Mixed-Integer Optimization. Fundamentals and Applications. *J. Glob. Optim.* 12, 1 (1998), 108–110. <https://doi.org/10.1023/A:1008256302713>

[36] Mohammadreza Pourreza, Hailong Li, Ruoxi Sun, Yeounoh Chung, Shayan Talaei, Gaurav Tarlok Kakkar, Yu Gan, Amin Saberi, Fatma Ozcan, and Sercan Ö. Arik. 2024. CHASE-SQL: Multi-Path Reasoning and Preference Optimized Candidate Selection in Text-to-SQL. *CoRR* abs/2410.01943 (2024). <https://doi.org/10.48550/ARXIV.2410.01943>

ARXIV.2410.01943 arXiv:2410.01943

[37] Haoran Qiu, Weichao Mao, Archit Patke, Shengkun Cui, Saurabh Jha, Chen Wang, Hubertus Franke, Zbigniew T. Kalbarczyk, Tamer Basar, and Ravishankar K. Iyer. 2024. Efficient Interactive LLM Serving with Proxy Model-based Sequence Length Prediction. *CoRR* abs/2404.08509 (2024). <https://doi.org/10.48550/ARXIV.2404.08509> arXiv:2404.08509

[38] Stuart Russell and Peter Norvig. 2020. *Artificial Intelligence: A Modern Approach (4th Edition)*. Pearson. <http://aima.cs.berkeley.edu/>

[39] Alexander Schrijver. 1998. *Theory of Linear and Integer Programming*. Wiley-Interscience.

[40] Jay Shah, Ganesh Bikshandhi, Ying Zhang, Vijay Thakkar, Pradeep Ramani, and Tri Dao. 2024. FlashAttention-3: Fast and Accurate Attention with Asynchrony and Low-precision. *CoRR* abs/2407.08608 (2024). <https://doi.org/10.48550/ARXIV.2407.08608> arXiv:2407.08608

[41] Foteini Strati, Sara McAllister, Amar Phanishayee, Jakub Tarnawski, and Ana Klimovic. 2024. DéjàVu: KV-cache Streaming for Fast, Fault-tolerant Generative LLM Serving. In *Forty-first International Conference on Machine Learning, ICML 2024, Vienna, Austria, July 21-27, 2024*. OpenReview.net. <https://openreview.net/forum?id=AbGbzGZYOD>

[42] Immanuel Trummer. 2022. DB-BERT: A Database Tuning Tool that "Reads the Manual". In *SIGMOD '22: International Conference on Management of Data, Philadelphia, PA, USA, June 12 - 17, 2022*, Zachary G. Ives, Angela Bonifati, and Amr El Abbadi (Eds.). ACM, 190–203. <https://doi.org/10.1145/3514221.3517843>

[43] Ashish Vaswani, Noam Shazeer, Niki Parmar, Jakob Uszkoreit, Llion Jones, Aidan N. Gomez, Łukasz Kaiser, and Illia Polosukhin. 2017. Attention is All you Need. In *Advances in Neural Information Processing Systems 30: Annual Conference on Neural Information Processing Systems 2017, December 4-9, 2017, Long Beach, CA, USA*, Isabelle Guyon, Ulrike von Luxburg, Samy Bengio, Hanna M. Wallach, Rob Fergus, S. V. N. Vishwanathan, and Roman Garnett (Eds.). 5998–6008.

[44] Jiale Xu, Rui Zhang, Cong Guo, Weiming Hu, Zihan Liu, Feiyang Wu, Yu Feng, Shixuan Sun, Changxu Shao, Yuhong Guo, Junping Zhao, Ke Zhang, Minyi Guo, and Jingwen Leng. 2024. vTensor: Flexible Virtual Tensor Management for Efficient LLM Serving. *CoRR* abs/2407.15309 (2024). <https://doi.org/10.48550/ARXIV.2407.15309> arXiv:2407.15309

[45] Gyeong-In Yu, Joo Seong Jeong, Geon-Woo Kim, Soojeong Kim, and Byung-Gon Chun. 2022. Orca: A Distributed Serving System for Transformer-Based Generative Models. In *16th USENIX Symposium on Operating Systems Design and Implementation, OSDI 2022, Carlsbad, CA, USA, July 11-13, 2022*, Marcos K. Aguilera and Hakim Weatherspoon (Eds.). USENIX Association, 521–538.

[46] Zhihang Yuan, Yuzhang Shang, Yang Zhou, Zhen Dong, Zhe Zhou, Chenhao Xue, Bingzhe Wu, Zhikai Li, Qingyi Gu, Yong Jae Lee, Yan Yan, Beidi Chen, Guangyu Sun, and Kurt Keutzer. 2024. LLM Inference Unveiled: Survey and Roofline Model Insights. *CoRR* abs/2402.16363 (2024). <https://doi.org/10.48550/ARXIV.2402.16363> arXiv:2402.16363

[47] Matei Zaharia, Omar Khattab, Lingjiao Chen, Jared Quincy Davis, Heather Miller, Chris Potts, James Zou, Michael Carbin, Jonathan Frankle, Naveen Rao, and Ali Ghodsi. 2024. The Shift from Models to Compound AI Systems. *The Berkeley Artificial Intelligence Research Blog*. <https://bair.berkeley.edu/blog/2024/02/18/compound-ai-systems/>.

[48] Lianmin Zheng, Wei-Lin Chiang, Ying Sheng, Tianle Li, Siyuan Zhuang, Zhanhao Wu, Yonghao Zhuang, Zhuohan Li, Zi Lin, Eric P Xing, et al. 2023. Lmsys-chat-1m: A large-scale real-world llm conversation dataset. *arXiv preprint arXiv:2309.11998* (2023).

[49] Lianmin Zheng, Liangsheng Yin, Zhiqiang Xie, Jeff Huang, Chuyue Sun, Cody Hao Wu, Shiyi Cao, Christos Kozyrakis, Ion Stoica, Joseph E. Gonzalez, Clark W. Barrett, and Ying Sheng. 2023. Efficiently Programming Large Language Models using SGLang. *CoRR* abs/2312.07104 (2023). <https://doi.org/10.48550/ARXIV.2312.07104> arXiv:2312.07104

[50] Zangwei Zheng, Xiaozhe Ren, Fuzhao Xue, Yang Luo, Xin Jiang, and Yang You. 2023. Response Length Perception and Sequence Scheduling: An LLM-Empowered LLM Inference Pipeline. In *Advances in Neural Information Processing Systems 36: Annual Conference on Neural Information Processing Systems 2023, NeurIPS 2023, New Orleans, LA, USA, December 10 - 16, 2023*, Alice Oh, Tristan Naumann, Amir Globerson, Kate Saenko, Moritz Hardt, and Sergey Levine (Eds.).

[51] Tianyang Zhong, Zhengliang Liu, Yi Pan, Yutong Zhang, Yifan Zhou, Shizhe Liang, Zihao Wu, Yanjun Lyu, Peng Shu, Xiaowei Yu, Chao Cao, Hanqi Jiang, Hanxu Chen, Yiwei Li, Junhao Chen, Huawen Hu, Yihen Liu, Huaqin Zhao, Shaochen Xu, Haixing Dai, Lin Zhao, Ruidong Zhang, Wei Zhao, Zhenyuan Yang, Jingyuan Chen, Peilong Wang, Wei Ruan, Hui Wang, Huan Zhao, Jing Zhang, Yiming Ren, Shihuan Qin, Tong Chen, Jiaxi Li, Arif Hassan Zidan, Afrar Jahin, Minheng Chen, Sichen Xia, Jason Holmes, Yan Zhuang, Jiaqi Wang, Bochen Xu, Weiran Xia, Jichao Yu, Kaibo Tang, Yaxuan Yang, Bolun Sun, Tao Yang, Guoyu Lu, Xianqiao Wang, Lilong Chai, He Li, Jin Lu, Lichao Sun, Xin Zhang, Bao Ge, Xintao Hu, Lian Zhang, Hua Zhou, Lu Zhang, Shu Zhang, Ninghao Liu, Bei Jiang, Linglong Kong, Zhen Xiang, Yudan Ren, Jun Liu, Xi Jiang, Yu Bao, Wei Zhang, Xiang Li, Gang Li, Wei Liu, Dinggang Shen, Andrea Sikora, Xiaoming Zhai, Dajiang Zhu, and Tianming Liu. 2024. Evaluation of OpenAI 01: Opportunities and Challenges of AGI. *CoRR* abs/2409.18486 (2024). <https://doi.org/10.48550/ARXIV.2409.18486> arXiv:2409.18486

[52] Yimin Zhong, Shengyu Liu, Junda Chen, Jianbo Hu, Yibo Zhu, Xuanzhe Liu, Xin Jin, and Hao Zhang. 2024. DistServe: Disaggregating Prefill and Decoding for Goodput-optimized Large Language Model Serving. In *18th USENIX Symposium on Operating Systems Design and Implementation, OSDI 2024, Santa Clara, CA, USA, July 10-12, 2024*, Ada Gavrilovska and Douglas B. Terry (Eds.). USENIX Association, 193–210.

[53] Xuanhe Zhou, Guoliang Li, and Zhiyuan Liu. 2023. LLM As DBA. *CoRR* abs/2308.05481 (2023). <https://doi.org/10.48550/ARXIV.2308.05481> arXiv:2308.05481

[54] Kan Zhu, Yilong Zhao, Liangyu Zhao, Gefei Zuo, Yile Gu, Dedong Xie, Yufei Gao, Qinyu Xu, Tian Tang, Zihao Ye, et al. 2024. NanoFlow: Towards Optimal Large Language Model Serving Throughput. *arXiv preprint arXiv:2408.12757* (2024).